Electrophile-Promoted Carbyne–CO Coupling at a Tantalum Center

John D. Protasiewicz, Brian S. Bronk, Axel Masschelein, and Stephen J. Lippard*

Department of Chemistry, Massachusetts Institute of Technology, Cambridge, Massachusetts 02139

Received October 6, 1993®

Siloxycarbyne complexes of the type [Ta(≡COSiR_3)(CO)(dmpe)$_2$], R_3 = ^{t}BuPh$_2$ (**1b**) or Ph$_3$ (**1c**), have been prepared by routes analogous to those previously described for [Ta(≡COSi-^{i}Pr$_3$)(CO)(dmpe)$_2$] (**1a**). Compounds **1a–c** react with R′$_3$SiCl to afford the acetylene complexes [Ta(R_3SiOC≡COSiR′$_3$)(dmpe)$_2$Cl] (R_3 = ^{i}Pr$_3$, R′$_3$ = Me$_3$ (**2a**); R_3 = ^{t}BuPh$_2$, R′$_3$ = Me$_3$ (**2b**); R_3 = Ph$_3$, R′$_3$ = Me$_3$ (**2c**); R_3 = ^{t}BuPh$_2$, R′$_3$ = Et$_3$ (**2d**)). The mechanism of C—C bond formation in these systems has been elucidated by stopped-flow kinetic studies of the reaction of **1a** with excess Me$_3$SiCl in THF to form **2a**. Addition of (*n*-pentyl)$_4$NCl increased the rate of reaction between **1a** and excess Me$_3$SiCl, but produced [Ta(Me$_3$SiOC≡COSiMe$_3$)(dmpe)$_2$Cl] rather than **2a**. A pathway for chloride-induced exchange of silyl groups between the starting material and excess Me$_3$SiCl has been elucidated. Addition of (*n*-butyl)$_4$NBPh$_4$ also strongly accelerated the observed reaction rates, but in this case the product formed was **2a**. The observed rate increases were attributed to an increase in the ionic strength of the solution. At a constant salt concentration of 23.9 mM (*n*-butyl)$_4$NBPh$_4$, the reaction was first order in both **1a** and Me$_3$SiCl, with a second order rate constant of 1.71 ± 0.04 M^{-1} s^{-1} at 22 ± 1 °C. These results are consistent with a mechanism involving electrophilic attack by the silyl reagent on the CO ligand of 1 as the rate-determining step of the reaction. Addition of AlEt$_3$ to **1b** allowed the isolation of [Ta(≡COSi^{t}BuPh$_2$)(COAlEt$_3$)(dmpe)$_2$] (**3b**), a model for the initial species formed upon silylation of the CO ligand in **1b**. Comparison of the spectroscopic and structural properties of **3b** with those of **1b** revealed that C—C bond formation does not occur upon addition of this particular Lewis acid. The structure of **3b** revealed several important features, the most significant of which is a decrease in the C—Ta—C angle to 73.4(4)° from the value of 89.1(3)° in **1b**. The corresponding angle in the reductively coupled product, [Ta(Et$_3$SiOC≡COSi^{t}BuPh$_2$)(dmpe)$_2$-Cl] (**2d**), the structure of which is also reported, is 36.5(2)°.

Introduction

Compounds having transition metal–carbon triple bonds undergo a variety of bond-forming and bond-breaking reactions.[1-3] In one important class of such reactions, the carbyne unit is coupled to an adjacent carbon monoxide or isocyanide ligand.[4-6] Nucleophile-induced carbyne–CO coupling was first discovered by Kreissl in 1976 during the reaction of [CpW(≡CTol)(CO)$_2$] with 2 equiv of PMe$_3$ (Scheme 1).[7] The intermediate η^2-ketenyl complex was subsequently prepared by removal of one of the PMe$_3$ ligands from the η^1-ketenyl product or by addition of 1 equiv of PMe$_3$ to [CpW(≡CTol)(CO)$_2$].[8-10] Following this pioneering work, many other examples of both nucleophile- and photochemical-induced coupling of carbyne and CO ligands to form η^2-ketenyl complexes have been reported.[11]

Scheme 1

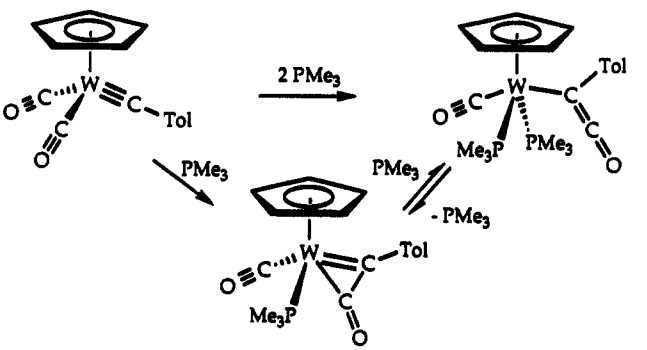

Conversion of an η^2-ketenyl to an acetylene ligand may be accomplished by addition of an appropriate alkylating reagent or electrophile to the oxygen atom. The scope and generality of acetylene formation by this route from one class of well-characterized [CpW(CO)(L)(η^2-RCC=O)] complexes is summarized in Scheme 2.[4]

In contrast to the many examples of base-promoted carbyne–CO coupling reactions, no definitive examples of electrophile-promoted carbyne–CO coupling have been reported. It was suggested, however, that coordination of AlCl$_3$ or AlMe$_3$ to a CO ligand during the reaction of

• Abstract published in *Advance ACS Abstracts*, February 1, 1994.

(1) Fischer, H.; Hofmann, P.; Kreissl, F. R.; Schrock, R. R.; Schubert, U.; Weiss, K. *Carbyne Complexes*; VCH Publishers: New York, 1988.
(2) Nugent, W. A.; Mayer, J. M. *Metal-Ligand Multiple Bonds: The Chemistry of Transition Metal Complexes Containing Oxo, Nitrido, Imido, Alkylidene, or Alkylidyne Ligands*; Wiley: New York, 1988.
(3) Kim, H. P.; Angelici, R. J. *Adv. Organomet. Chem.* **1987**, *27*, 51.
(4) Mayr, A.; Bastos, C. M. *Prog. Inorg. Chem.* **1992**, *40*, 1.
(5) Mayr, A.; Hoffmeister, H. *Adv. Organomet. Chem.* **1991**, *32*, 227.
(6) Mayr, A. *Comments Inorg. Chem.* **1990**, *10*, 227.
(7) Kreissl, F. R.; Frank, A.; Schubert, U.; Lindner, T. L.; Huttner, G. *Angew. Chem., Int. Ed. Engl.* **1976**, *15*, 632.
(8) Kreissl, F. R.; Eberl, K.; Uedelhoven, W. *Chem. Ber.* **1977**, *110*, 3782.
(9) Uedelhoven, W.; Eberl, K.; Kreissl, F. R. *Chem. Ber.* **1979**, *112*, 3376.
(10) Sieber, W. J.; Wolfgruber, M.; Trsan-Huy, N. H.; Schmidt, H. R.; Heiss, H.; Hofmann, P.; Kreissl, F. R. *J. Organomet. Chem.* **1988**, *340*, 341.
(11) For an early review of ketenyl complexes see: Geoffroy, G. L.; Bassner, S. L. *Adv. Organomet. Chem.* **1988**, *28*, 1.

0276-7333/94/2313-1300$04.50/0

Scheme 2

$$[CpW(L)(CO)(\eta^2\text{-}RCC{=}O)]^m \xrightarrow{\text{electrophile}} [CpW(L)(CO)(RC{\equiv}COE)]^n$$

E = R^+, H^+, or XY_3

L	m	n	electrophile
CN	-1	0	Me_3OBF_4
PMe_3	0	+1	Me_3OBF_4, MeOTf, Et_3OBF_4, HBF_4
PMe_3	0	0	$AlEt_3$, $AlCl_3$, $InCl_3$, BCl_3, borane

$[W(\equiv CH)(PMe_3)_4Cl]$ with CO might have promoted such a coupling reaction (eq 1).[12,13] No intermediates were isolated or detected in this interesting reaction, however.

$$[W(\equiv CH)(PMe_3)_4Cl] \xrightarrow[30\ \text{psig CO}]{AlX_3} W(HC{\equiv}COAlX_3)(CO)(PMe_3)_3Cl \quad (1)$$

$$AlX_3 = AlMe_3 \text{ or } AlCl_3$$

Our interest in carbyne–CO coupling arose during an investigation of the mechanism of the reaction between two CO ligands in low valent niobium and tantalum complexes. A coordinated acetylene product forms in this chemistry, and we have referred to the overall reaction, illustrated in eq 2, as reductive coupling (dmpe = 1,2 bis-

$$[M(CO)_2(dmpe)_2X] \xrightarrow{\text{reductant}} \xrightarrow{2R_3SiX} [M(R_3SiOC{\equiv}COSiR_3)(dmpe)_2X] \quad (2)$$

$$M = Nb \text{ or } Ta$$

$$X = Cl, I, \text{ or } OTf$$

(dimethylphosphino)ethane).[14] In the first step of this reaction (Scheme 3), the seven-coordinate M(I) precursor is converted to a M(–I) dicarbonyl anion.[15] Much of the electron density in this highly reduced complex is delocalized out onto the two CO ligands, as demonstrated by the low frequency CO stretching bands, 1663 and 1561 cm^{-1}, in the IR spectrum of the tantalum derivative. Electrophilic attack by R_3SiX on this anionic complex generates a siloxycarbyne complex in the next step of the reaction mechanism. The stretching frequency for the terminal CO ligand in this complex occurs at approximately 1760–1800 cm^{-1}. Carbon–carbon bond formation takes place following addition of R_3SiX to the carbyne–CO complexes, generating a bis(siloxyacetylene) ligand. Similar highly reduced and carbyne/carbonyl intermediates have been isolated in the reductive coupling of CO and CNR ligands in $[Ta(CO)(CNR)(dmpe)_2Cl]$, and proposed in the coupling of two isocyanide ligands in $[Ta(CNMe)_2(dmpe)_2Cl]$[16,17] and $[M(CNR)_6]$ (M = Cr, Mo, and W).[18–20]

Scheme 3

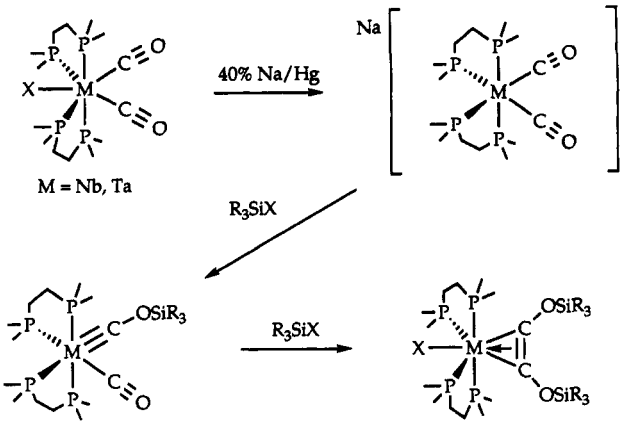

Scheme 4

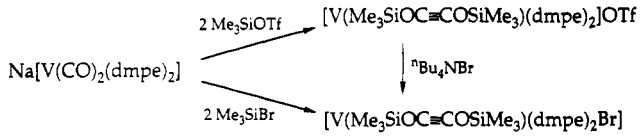

During investigations of the related vanadium system, we discovered that addition of 2 equiv of Me_3SiOTf to $Na[V(CO)_2(dmpe)_2]$ yielded a coupled product in which, unlike the tantalum system, the triflate counterion was not coordinated to the metal center (Scheme 4).[21] Addition of bromide ion to this 16 e^- species produced $[V(Me_3SiOC{\equiv}COSiMe_3)(dmpe)_2Br]$, which could also be directly prepared from the vanadium anion by addition of 2 equiv of Me_3SiBr. Coupling of the carbyne–CO ligands in $[V(\equiv COSiMe_3)(CO)(dmpe)_2]$ upon reaction with Me_3SiOTf thus appeared to be an unprecedented case of a purely electrophile-induced carbyne–CO coupling reaction.

Such an interpretation, however, implies that a terminal CO ligand with a stretching frequency of 1750–1800 cm^{-1} could be alkylated at oxygen, a reaction having little precedence apart from the aforementioned R_3SiX silylation of the $[M(CO)_2(dmpe)_2]^-$ anions, which have much lower CO stretching frequencies. Moreover, we had previously suggested that high coordinate complexes might be necessary for reductive coupling to occur, since the isolated products were all seven-coordinate species, taking the acetylene ligand as occupying two coordination sites.[22] This requirement could be fulfilled for the vanadium system if addition of a nucleophile to the carbyne species to generate an η^2-ketenyl intermediate (an example of a seven-coordinate complex) had occurred prior to formation of the C≡C bond.

In order to investigate these issues further, a kinetic analysis of the reaction of the Me_3SiCl-promoted carbyne–CO coupling has been carried out. In addition, we have studied the reaction with a different electrophile, $AlEt_3$, in order to gain further insight into the reaction mechanism. In the present article we report the full details of these kinetic, spectroscopic, and structural studies which address the intimate details of the coupling of the carbyne and CO ligands in complexes of the type [Ta(≡CO-

(12) Churchill, M. R.; Wasserman, H. J.; Holmes, S. J.; Schrock, R. R. *Organometallics* **1982**, *1*, 766.
(13) Holmes, S. J.; Schrock, R. R.; Churchill, M. R.; Wasserman, H. J. *Organometallics* **1984**, *3*, 476.
(14) Vrtis, R. N.; Lippard, S. J. *Isr. J. Chem.* **1990**, *30*, 331.
(15) Vrtis, R. N.; Liu, S.; Rao, C. P.; Bott, S. G.; Lippard, S. J. *Organometallics* **1991**, *10*, 275.
(16) Carnahan, E. M.; Lippard, S. J. *J. Am. Chem. Soc.* **1992**, *114*, 4166.
(17) Carnahan, E. M.; Lippard, S. J. *J. Am. Chem. Soc.* **1990**, *112*, 3230.
(18) Carnahan, E. M.; Lippard, S. J. *J. Chem. Soc., Dalton Trans.* **1991**, 699.
(19) Filippou, A. C.; Grünleitner, W.; Völkl, C.; Kiprof, P. *Angew. Chem., Int. Ed. Engl.* **1991**, *30*, 1167.
(20) Acho, J. A.; Lippard, S. J. *Organometallics*, preceding paper in this issue.
(21) Protasiewicz, J. D.; Lippard, S. J. *J. Am. Chem. Soc.* **1991**, *113*, 6564.
(22) Carnahan, E. M.; Protasiewicz, J. D.; Lippard, S. J. *Acc. Chem. Res.* **1993**, *26*, 90.

$SiR_3)(CO)(dmpe)_2$] during reaction with Me_3SiCl and other electrophiles.[23]

Experimental Section

General Considerations. All reactions and manipulations were carried out under a nitrogen atmosphere by using standard Schlenk techniques or a Vacuum Atmospheres drybox. The compounds $[Ta(CO)_2(dmpe)_2Cl]$, $[Ta(\equiv COSi^iPr_3)(CO)(dmpe)_2]$ (**1a**), $[Ta(^iPr_3SiOC\equiv COSiMe_3)(dmpe)_2Cl]$ (**2a**), and $[Ta(Me_3SiOC\equiv COSiMe_3)(dmpe)_2Cl]$ were prepared by published procedures.[15,24] Isotopically-enriched $[Ta(^{13}CO)_2(dmpe)_2Cl]$ was prepared by the same method used for $[Ta(CO)_2(dmpe)_2Cl]$ except that an atmosphere of ^{13}CO (Cambridge Isotopes, 99% ^{13}C enriched) was used, replacing CO. Solvents (THF, pentane, toluene, diethyl ether, and DME) were distilled under nitrogen from sodium benzophenone ketyl. C_6D_6 was dried by passage through a column of alumina and stored under nitrogen. Me_3SiCl employed in the kinetic studies was distilled from 1,8-bis(dimethylamino)naphthalene (proton sponge) under nitrogen using silylated glassware and stored in the drybox. $(n\text{-butyl})_4NBPh_4$ and $(n\text{-pentyl})_4NCl$ were dried under high vacuum above 100 °C. All other reagents were used as received after degassing. Proton chemical shifts were referenced to residual solvent peaks. ^1H and $^{31}P\{^1H\}$ NMR spectra were recorded on a Varian XL300 instrument. $^{31}P\{^1H\}$ NMR spectra are referenced to external phosphoric acid.

$[Ta(\equiv COSi^tBuPh_2)(CO)(dmpe)_2]$ (1b). A solution of 0.112 g (0.196 mmol) of $[Ta(CO)_2(dmpe)_2Cl]$ in 15 mL of THF was rapidly stirred with excess 40% Na/Hg for 5 h to generate $Na[Ta(CO)_2(dmpe)_2]$. This solution was decanted into another flask, and 46 μL (0.177 mmol) of $^tBuPh_2SiCl$ was added by syringe. The solution slowly turned deep red and was allowed to stir for 10 min. The solvent was removed under vacuum, and the red product was triturated twice with pentane and then extracted with 15 mL of pentane. Removal of the pentane yielded 0.138 g of a red microcrystalline product, **1b**, displaying a single ν_{CO} band at 1793 cm^{-1} in its FTIR spectrum. This material was further purified by recrystallization from pentane at −30 °C to yield 0.089 g (54%) of **1b**. ^1H NMR (C_6D_6): δ 8.10 (m, 4 H), 7.34 (m, 4 H), 7.24 (m, 2 H), 1.65 (d, J_{HP} = 6.6 Hz, 3 H), 1.46 (d, J_{HP} = 7.2 Hz, 3 H), 1.44 (d, J_{HP} = 6.0 Hz, 3 H), 1.41 (d, J_{HP} = 4.2 Hz, 3 H), 1.28 (d, J_{HP} = 5.1 Hz, 3H), 1.25 (s, 9H), 1.17 (d, J_{HP} = 3.3 Hz, 3 H), 0.92 (d, J_{HP} = 3.3 Hz, 3H), 0.61 (d, J_{HP} = 3.6 Hz, 3 H), 1.6–0.6 (8H, dmpe methylene protons). $^{31}P\{^1H\}$ NMR (C_6D_6): δ 25.6 (m), 12.2 (m), −1.0 (m). IR (Nujol): 1793 (s), 1274 (s), 1110 (m), 927 (m), 885 (w), 814 (m), 698 (m) cm^{-1}. Anal. Calcd for $C_{30}H_{51}O_2P_4SiTa$: C, 46.39; H, 6.62; N, 0.00. Found: C, 46.08; H, 6.66; N, 0.00.

$[Ta(\equiv COSiPh_3)(CO)(dmpe)_2]$ (1c). A solution of 0.600 g (1.05 mmol) of $[Ta(CO)_2(dmpe)_2Cl]$ in 15 mL of THF was rapidly stirred with excess 40% Na/Hg for 6 h to generate $Na[Ta(CO)_2(dmpe)_2]$. This solution was decanted into another flask, and 0.310 g (1 equiv) of Ph_3SiCl was added. The solution quickly turned deep red and was allowed to stir for 1.5 h. The solvent was removed under vacuum, and the red product was triturated twice with pentane and then recrystallized from diethyl ether (−30 °C). Two crops of crystals yielded 0.564 g of **1c**, 67%. ^1H NMR (C_6D_6): δ 8.00 (m, 6H), 7.23 (m, 9H), 1.65 (d, J_{HP} = 7.2 Hz, 3H), 1.47 (d, J_{HP} = 6.6 Hz, 3H), 1.36 (d, J_{HP} = 3.9 Hz, 3H), 1.28 (d, J_{HP} = 5.7 Hz, 6H), 1.16 (d, J_{HP} = 3.6 Hz, 3H), 0.90 (d, J_{HP} = 3.0 Hz), 0.60 (d, J_{HP} = 3.6 Hz, 3H), 1.6–0.6 (8H, dmpe methylene protons). $^{31}P\{^1H\}$ NMR (C_6D_6): δ 25.2 (m), 12.0 (m), −1.1 (m). IR (Nujol): 1761 (s), 1252 (s), 1186 (w), 1112 (m), 993 (w), 928 (m), 885 (w), 819 (m), 742 (w), 695 (m), 632 (w) cm^{-1}. Anal. Calcd for $C_{32}H_{47}O_2P_4SiTa$: C, 48.25; H, 5.95; N, 0.00. Found: C, 48.09; H, 6.02; N. 0.00.

$[Ta(Me_3SiOC\equiv COSi^tBuPh_2)(dmpe)_2Cl]$ (2b). A solution of 0.121 g (0.211 mmol) of $[Ta(CO)_2(dmpe)_2Cl]$ in 15 mL of THF was rapidly stirred with excess 40% Na/Hg for 4 h to generate $Na[Ta(CO)_2(dmpe)_2]$. This solution was decanted into another flask, and 55 μL (1 equiv) of $^tBuPh_2SiCl$ was added by syringe. The solution quickly turned deep red and was allowed to stir for 3 h. The solvent was removed under vacuum, and the red product was triturated with pentane and then extracted with 15 mL of pentane. The pentane was then removed, the red solid was taken up into 10 mL of THF and 26 μL of Me_3SiCl (1 equiv) added, and the solution was allowed to stir overnight. The solvent was removed under vacuum and the product recrystallized from 15 mL of pentane (−30 °C) to yield 0.107 g of **2b**. ^1H NMR (C_6D_6): δ 7.76 (m, 4H), 7.21 (m, 6H), 1.63 (s, 12H), 1.60 (br m, 8H), 1.52 (s, 12H), 1.11 (s, 9H), −0.44 (s, 9H). ^1H NMR (THF-d_8): δ 7.67 (m, 4H), 7.23 (m, 6H), 1.7 (br m, 8H), 1.67 (s, 12H), 1.45 (s, 12H), 0.93 (s, 9H), −0.65 (s, 9 H). $^{31}P\{^1H\}$ NMR (C_6D_6): δ 28.0 (s). IR (Nujol): 1565 (m), 1300 (w), 1280 (w), 1252 (w), 1143 (s), 1115 (w), 1054 (m), 930 (s), 892 (m), 840 (m), 731 (s), 701 (m) cm^{-1}. Anal. Calcd for $C_{29}H_{58}O_2P_4SiClTa$: C, 44.78; H, 6.83; N, 0.00. Found: C, 44.93; H, 6.85; N, 0.00.

$[Ta(Me_3SiOC\equiv COSiPh_3)(dmpe)_2Cl]$ (2c). A 25-mL, one-necked pear-shaped flask fitted with a rubber septum was charged with **1c** (0.104 g, 0.13 mmol) and 10 mL of THF. Upon dissolution, $^nBu_4NBPh_4$ (0.146 g, 0.26 mmol) was added, followed by Me_3SiCl (0.017 mL, 0.015 g, 0.13 mmol) in a single portion via syringe. The reaction mixture was allowed to stir for 4 h, during which time the color changed from deep red to green/brown. The solvents were removed under vacuum, the product was extracted with 20 mL of pentane, and the pentane was removed under vacuum. After trituration with two 10-mL portions of pentane, the product was crystallized from pentane at −30 °C to afford 0.088 g (75%) of **2c**. IR (Nujol): 1592 (m), 1417 (w), 1377 (m), 1288 (w), 1246 (w), 1122 (s), 1114 (s), 1101 (m), 1047 (s), 1028 (m), 937 (s), 925 (s), 890 (m), 840 (s), 728 (m), 710 (s), 697 (s), 623 (m) cm^{-1}. ^1H NMR (300 MHz, C_6D_6): δ 7.80–7.83 (m, 6H), 7.19–7.21 (m, 9H), 1.29–1.65 (m, 32H), −0.07 (s, 9H). ^{31}P NMR (121 MHz, C_6D_6): δ 22.7. Anal. Calcd for $C_{35}H_{56}O_2P_4Si_2ClTa$: C, 46.44; H, 6.23; N, 0.00. Found: C. 46.74; H, 6.44; N, 0.00.

$[Ta(Et_3SiOC\equiv COSi^tBuPh_2)(dmpe)_2Cl]$ (2d). Method A. A 25-mL, one-necked pear-shaped flask fitted with a rubber septum was charged with **1b** (0.155 g, 0.20 mmol) and 10 mL of THF. Upon dissolution, Et_3SiCl (0.034 mL, 0.030 g, 0.20 mmol) was added by syringe. The reaction mixture was allowed to stir for 24 h, during which time the color changed from deep red to green/brown. The solvents were removed under vacuum, the product was extracted with 10 mL of pentane and the solution was filtered, and the pentane was removed under vacuum. Crystallization from pentane at −30 °C provided 0.138 g (75%) of **2d**.

Method B. A 25-mL, one-necked pear-shaped flask fitted with a rubber septum was charged with **1b** (0.155 g, 0.20 mmol) and 10 mL of THF. Upon dissolution, $^nBu_4NBPh_4$ (0.202 g, 0.36 mmol) was added, followed by Et_3SiCl (0.034 mL, 0.030 g, 0.20 mmol) in one portion via syringe. The reaction mixture was allowed to stir for 70 min, during which time the color changed from deep red to green/brown. The solvents were removed under vacuum, the product was extracted with 20 mL of pentane, and the pentane was removed under vacuum. After trituration with two 10-mL portions of pentane, the product was crystallized from pentane at −30 °C, to afford 0.148 g (80%) of **2d**. IR (Nujol): 1559 (m), 1412 (m), 1289 (w), 1112 (s), 1032 (s), 938 (s), 889 (s), 819 (w), 743 (m), 732 (m), 700 (s), and 624 (m) cm^{-1}. ^1H NMR (300 MHz, C_6D_6): δ 7.80–7.83 (m, 4H), 7.22–7.24 (m, 6H), 1.41–1.58 (m, 8H), 1.59 (bs, 12H), 1.50 (bs, 12H), 1.10 (s, 9H), 0.73 (t, J = 8.1 Hz). ^{31}P NMR (121 MHz, C_6D_6): δ 27.1. Anal. Calcd for $C_{36}H_{66}O_2P_4Si_2ClTa$: C, 46.63; H, 7.17; N, 0.00. Found: C, 46.68; H, 7.19; N, 0.00.

$[Ta(\equiv COSi^iPr_3)(COAlEt_3)(dmpe)_2]$ (3a). This compound was prepared in solution but not isolated. To a solution of 0.046 g (0.066 mmol) of **1a** in toluene (for study by infrared spectroscopy) or C_6D_6 (for study by NMR spectroscopy) was added 9.5

(23) An initial report of this work has appeared. See: Protasiewicz, J. D.; Masschelein, A.; Lippard, S. J. *J. Am. Chem. Soc.* **1993**, *115*, 808.

(24) Protasiewicz, J. D.; Bianconi, P. A.; Williams, I. D.; Liu, S.; Rao, C. P.; Lippard, S. J. *Inorg. Chem.* **1992**, *31*, 4134.

Table 1. Crystallographic Information for [Ta(≡COSi^{t}BuPh$_2$)(CO)(dmpe)$_2$] (1b) [Ta(Et$_3$SiOC≡COSi^{t}BuPh$_2$)(dmpe)$_2$Cl] (2d), and [Ta(≡COSi^{t}BuPh$_2$)(COAlEt$_3$)(dmpe)$_2$] (3b)[a]

	1b	2d	3b
a (Å)	30.494(5)	19.258(2)	21.147(4)
b (Å)	10.568(1)	12.506(2)	13.357(2)
c (Å)	22.366(4)	20.213(2)	32.780(6)
α (deg)			
β (deg)	92.876(9)	116.098(9)	105.14(1)
γ (deg)			
V (Å^3)	7198(2)	4371(1)	8937(3)
T (°C)	–78	–72	–47
fw	776.66	927.38	890.82
Z	8	4	8
ρ_{calc} (g cm^{-3})	1.43	1.41	1.32
space group	$C2/c$	$P2_1/c$	$C2/c$
2θ limits (deg)	3–50	3–50	3–48
data limits	$\pm h,+k,+l$	$\pm h,+k,+l$	$\pm h,+k,+l$
μ(cm^{-1})	32.5	27.7	26.4
total no. of data	7421	8710	8642
no. of unique data[b]	4496	6080	5171
no. of param	342	415	401
p factor	0.05	0.05	0.05
R^c	0.036	0.029	0.051
R_w	0.050	0.038	0.065

[a] Data were collected on an Enraf Nonius CAD-4F κ geometry diffractometer using Mo Kα radiation. [b] Observation criterion $I > 3\sigma(I)$. [c] $R = \sum||F_o| - |F_c||/\sum|F_o|$, $R_w = [\sum w(|F_o| - |F_c|)^2/\sum w|F_o|^2]^{1/2}$, where $w = 1/\sigma^2(F)$, as defined in: Carnahan, E. M.; Rardin, R. L.; Bott, S. G.; Lippard, S. J. *Inorg. Chem.* **1992**, *31*, 5193.

μL (0.069 mmol) of AlEt$_3$ by syringe. The IR spectrum indicated complete consumption of the starting carbyne complex, as evidenced by the loss of the CO stretch at 1790 cm^{-1}, and formation of a new complex, **3a**, with ν_{CO} = 1605 cm^{-1}. ^{1}H NMR (C$_6$D$_6$): δ 1.72–1.67 (m, 6H), 1.69 (t, J = 8.4 Hz, 9H), 1.40 (d, J_{HP} = 5.7 Hz, 3H), 1.38–1.16 (m, 34H), 1.14–0.80 (m, 4H), 0.72 (d, J_{HP} = 3.6 Hz, 3H), 0.58 (d, J_{HP} = 3.9 Hz, 3H), 0.46 (q, J = 8.3 Hz, 6H). ^{31}P{^{1}H} (C$_6$D$_6$): δ 21.9 (m), 4.0 (m), 1.8 (m).

[Ta(≡COSi^{t}BuPh$_2$)(COAlEt$_3$)(dmpe)$_2$] (3b). To a solution of 0.143 g (0.184 mmol) of **1b** in a mixture of 3 mL of toluene and 8 mL of pentane was added 28 μL (0.205 mmol) of AlEt$_3$ by syringe, which caused the solution to change immediately from deep red to a red-orange color. Shortly thereafter, small crystals of **3b** began to precipitate, and the solution was then placed in a –30 °C freezer to facilitate crystallization. After filtration and drying, **3b** was obtained in 77% yield (0.126 g). ^{1}H NMR (C$_6$D$_6$): δ 7.93 (m, 4H), 7.30 (m, 6H), 1.74 (t, 8 Hz, 9H), 1.53 (two overlapping doublets, 6H), 1.39 (d, J_{HP} = 6 Hz, 3H), 1.23 (s, 9H), 1.15 (d, J_{HP} = 3.9 Hz, 3H), 1.06 (d, J_{HP} = 3.6 Hz, 3H), 0.90 (d, J_{HP} = 5.7 Hz, 3H), 0.62–0.52 (m, overlap of two doublets and a quartet, 15H), 1.7–0.6 (8H, dmpe methylene protons). ^{31}P{^{1}H} (C$_6$D$_6$): δ 22.1 (m), 4.3 (br m), –1.9 (m). IR (Nujol): 1593 (s), 1321 (s), 1112 (w), 984 (w), 934 (m), 813 (m), 703 (m) cm^{-1}. Anal. Calcd for C$_{36}$H$_{66}$AlO$_2$P$_4$SiTa (**3b**): C, 48.54; H, 7.47; N, 0.00. Found: C, 48.86; H, 7.36; N, 0.00.

[Ta(≡COSiPh$_3$)(COAlEt$_3$)(dmpe)$_2$] (3c). The compound was prepared but not isolated from 0.043 g (0.054 mmol) of **1c** and 8 μL (0.059 mmol) of AlEt$_3$, following the procedure described for **3a**. ^{1}H NMR (C$_6$D$_6$): δ 7.91–7.86 (m, 6H), 7.30–7.18 (m, 9H), 1.71–1.64 (m, 12H), 1.7–0.6 (m, 8H), 1.54–1.47 (m, 6H), 1.41–1.38 (m, 3H), 1.14–1.13 (m, 3H), 1.13–1.03 (m, 3H), 0.80–0.78 (m, 3H), 0.61–0.60 (m, 3H), 0.52–0.49 (m, 6H). ^{31}P{^{1}H} (C$_6$D$_6$): δ 21.2 (m), 4.04 (m), 2.25 (m).

X-ray Crystallography. [Ta(≡COSi^{t}BuPh$_2$)(CO)(dmpe)$_2$] (1b). Red crystals were grown by cooling a saturated solution of **1b** in pentane to –30 °C. An irregularly shaped crystal of **1b** (dimensions 0.45 × 0.3 × 0.3 mm) was cut from a larger specimen and mounted on the end of a quartz fiber with silicon grease on a cold stage. Unit cell parameters and intensity data were obtained by methods standard in our laboratory, details of which are provided in Table 1. The crystal was judged to be acceptable on the basis of open counter ω-scans of several low angle reflections ($\Delta\bar{\omega}_{1/2}$ = 0.30°) and by axial photographs. An empirical absorption correction was applied to the data. The tantalum atom was located by direct methods. Remaining non-hydrogen atoms were revealed by subsequent least-squares refinements and difference Fourier maps. All non-hydrogen atoms were refined anisotropically, except for C21A and C21B. These two carbon atoms, which comprise methylene linkers of one of the dmpe ligands, were disordered over two sets of positions. A model accounting for this orientational disorder was introduced and refined. The relative occupancies were determined to be 60/40. Hydrogen atoms were placed at calculated positions in the final refinement cycles (H atoms were not generated for C21A and C21B). The largest residual peak in the final difference Fourier map was 2.6 e/Å^3, located near P2.

[Ta(Et$_3$SiC≡COSi^{t}BuPh$_2$)(dmpe)$_2$Cl] (2d). Green-brown crystals were grown by cooling a saturated solution of **2d** in pentane at –30 °C. An irregularly shaped crystal (dimensions 0.3 × 0.3 × 0.2 mm) was mounted on the end of a quartz fiber with silicon grease on a cold stage. Unit cell parameters and intensity data were obtained by methods standard in our laboratory, details of which are provided in Table 1. The crystal was judged to be acceptable on the basis of open counter ω-scans of a low angle reflection ($\Delta\bar{\omega}_{1/2}$ = 0.21°) and by axial photographs. The tantalum atom was located by direct methods. Remaining non-hydrogen atoms were revealed by subsequent least squares refinements and difference Fourier maps. All non-hydrogen atoms were refined anisotropically.

[Ta(≡COSi^{t}BuPh$_2$)(COAlEt$_3$)(dmpe)$_2$] (3b). Red crystals were grown by cooling a saturated solution of **3b** in a toluene–pentane mixture to –30 °C. An irregularly shaped crystal of **3b** (dimensions 0.45 × 0.35 × 0.3 mm) was cut from a larger specimen and mounted on the end of a quartz fiber with silicon grease on a cold stage. Unit cell parameters and intensity data were obtained by methods standard in our laboratory, details of which are provided in Table 1. The crystal was judged to be acceptable on the basis of open counter ω-scans of several low angle reflections ($\Delta\bar{\omega}_{1/2}$ = 0.25°) and by axial photographs. The tantalum atom was located by direct methods. Remaining non-hydrogen atoms were revealed by subsequent least squares refinements and difference Fourier maps. All non-hydrogen atoms were refined anisotropically, except for C21. This carbon atom, which is one of the methylene of one of the dmpe ligands, was found to exhibit large thermal parameters, presumably due to a disorder over two sites, as observed for **1b**. A model accounting for this disorder could not be found, however. Hydrogen atoms were placed at calculated positions in the final refinement cycles (H atoms were not generated for C21). The largest residual peak in the final difference Fourier map was 1.9 e/Å^3, located near the Ta atom.

Kinetics Experiments. THF solutions of **1a** and Me$_3$SiCl, with and without added tetraalkylammonium salts, were prepared in a glovebox and loaded into gastight syringes. The contents of the two syringes were rapidly mixed in a stopped-flow kinetic accessory (Applied Photophysics RX-1000, deadtime ≈ 15 ms) at room temperature (22 ± 1 °C) under strict absence of oxygen and water. The resulting transformations of the UV–visible absorption spectrum were recorded with a diode array spectrophotometer (HP 8452A) and the corresponding kinetic traces were monitored at 480 nm with a fast fiber-optics detection system (Oriel Corp.). Kinetic and spectral data were acquired through homemade software (Labview2 environment and interfaces, National Instruments) on a Macintosh IIfx computer (Apple Computer Inc.). Data treatment and analyses were performed on the same computer (Kaleidagraph, Synergy Software). Reported kinetic constants were determined by nonlinear least squares curve fitting according to a first order expression over at least 5 half-lives, 800 experimental points, and are the arithmetic mean of three consecutive runs.

Results and Discussion

Synthesis and Structure of Siloxycarbyne–CO Complexes and Their Reductively Coupled Products.

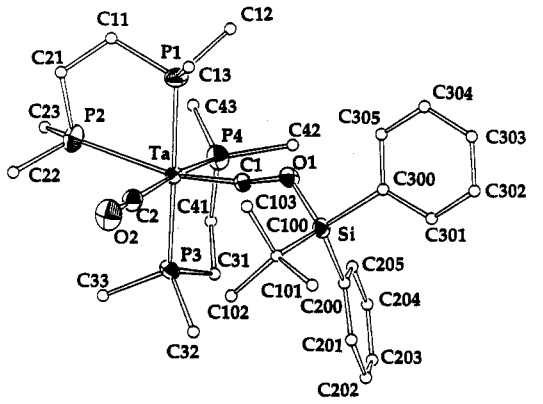

Figure 1. Structural diagram of [Ta(≡COSi^{t}BuPh$_2$)(CO)(dmpe)$_2$] (**1b**) showing 40% thermal ellipsoids for selected atoms and, for clarity, 0.1-Å spheres for the remaining non-hydrogen atoms. Disordered atom C21 having the higher site occupancy (see text) is depicted. A full ORTEP diagram is provided with the supplementary material for ref 23.

Table 2. Positional Parameters and *B*(eq) for [Ta(≡COSi^{t}BuPh$_2$)(CO)(dmpe)$_2$] (1b)[a]

atom	*x*	*y*	*z*	*B*(eq), Å^2 [b]
Ta	0.102660(8)	0.24554(2)	0.03843(1)	1.66(1)
P1	0.12054(7)	0.0177(2)	0.04106(9)	2.82(8)
P2	0.06044(7)	0.1632(2)	0.1295(1)	3.6(1)
P3	0.08960(6)	0.4791(2)	0.04849(8)	2.18(7)
P4	0.17107(6)	0.3209(2)	0.10002(9)	3.02(9)
Si	0.13980(6)	0.2956(2)	−0.15332(8)	2.08(8)
O1	0.1473(2)	0.2178(4)	−0.0888(2)	2.4(2)
O2	0.0095(2)	0.1935(6)	−0.0298(2)	4.3(3)
C1	0.1288(2)	0.2446(5)	−0.0360(3)	1.9(3)
C2	0.0439(2)	0.2130(7)	−0.0043(3)	2.8(3)
C11	0.0956(4)	−0.0721(8)	0.1013(4)	6.1(6)
C12	0.1783(3)	−0.0358(8)	0.0490(5)	5.6(5)
C13	0.1037(3)	−0.0735(8)	−0.0251(4)	4.8(5)
C21A	0.0552(5)	−0.018(2)	0.1216(7)	5.1(3)
C21B	0.0881(7)	0.004(2)	0.153(1)	4.5(5)
C22	0.0012(3)	0.180(2)	0.1275(5)	9.9(8)
C23	0.0712(4)	0.199(1)	0.2077(4)	9.7(8)
C31	0.1396(3)	0.5652(7)	0.0745(4)	4.0(4)
C32	0.0723(3)	0.5726(7)	−0.0170(4)	4.0(4)
C33	0.0511(3)	0.5359(8)	0.1024(4)	4.1(4)
C41	0.1649(3)	0.492(1)	0.1211(5)	6.1(6)
C42	0.2223(2)	0.324(1)	0.0629(4)	5.0(5)
C43	0.1894(3)	0.2562(9)	0.1722(4)	5.4(5)
C100	0.0818(2)	0.2775(7)	−0.1850(3)	2.7(3)
C101	0.0793(3)	0.3040(9)	−0.2523(3)	3.8(4)
C102	0.0499(2)	0.3627(8)	−0.1539(3)	3.5(4)
C103	0.0675(3)	0.1413(8)	−0.1751(4)	4.0(4)
C200	0.1573(2)	0.4640(6)	−0.1410(3)	2.3(3)
C201	0.1408(3)	0.5680(7)	−0.1731(3)	3.4(4)
C202	0.1545(3)	0.6900(8)	−0.1586(4)	4.5(4)
C203	0.1832(3)	0.7099(8)	−0.1121(4)	4.3(4)
C204	0.2013(3)	0.6099(8)	−0.0802(4)	3.6(4)
C205	0.1876(2)	0.4896(7)	−0.0939(3)	3.0(3)
C300	0.1781(2)	0.2077(6)	−0.2023(3)	2.1(3)
C301	0.1936(2)	0.2656(7)	−0.2538(3)	2.8(3)
C302	0.2189(3)	0.1989(8)	−0.2918(3)	3.3(4)
C303	0.2294(2)	0.0779(8)	−0.2809(3)	3.5(4)
C304	0.2144(2)	0.0188(7)	−0.2296(3)	3.4(4)
C305	0.1894(2)	0.0859(7)	−0.1918(3)	2.7(3)

[a] Atoms are labeled as indicated in Figure 1. Estimated standard deviations in the last digit are given in parentheses. [b] $B(\text{eq}) = {}^4/_3[a^2\beta_{11} + b^2\beta_{22} + c^2\beta_{33} + 2ab\cos(\gamma)\beta_{12} + 2ac\cos(\beta)\beta_{13} + 2bc\cos(\alpha)\beta_{23}]$.

Siloxycarbyne complexes of the type [Ta(≡COSiR$_3$)(CO)(dmpe)$_2$] were prepared by addition of the appropriate trialkylsilyl halide to THF solutions of Na[Ta(CO)$_2$(dmpe)$_2$] (eq 3).[15] Use of the sterically demanding silyl reagents is necessary, for addition of 1 equiv of a less hindered reagent (such as Me$_3$Si or Me$_2$PhSi) to Na[Ta(CO)$_2$(dmpe)$_2$] led to the isolation of dinuclear carbyne species of the form [(CO)(dmpe)$_2$Ta≡COTa(R$_3$SiOC≡COSiR$_3$)(dmpe)$_2$].[25,26] The synthesis and X-ray structure of [Ta(≡COSi^{i}Pr$_3$)(CO)(dmpe)$_2$] (**1a**) have been reported in earlier work. This siloxycarbyne complex displays ν_{CO} (Nujol) stretching bands at 1802 and 1311 cm^{-1}. The new complexes [Ta(≡COSi^{t}BuPh$_2$)(CO)(dmpe)$_2$] (**1b**) and [Ta(≡COSiPh$_3$)(CO)(dmpe)$_2$] (**1c**) were prepared for the present study by an analogous route. Their spectroscopic properties closely mimic those of **1a**, including the ν_{CO} (Nujol) values which for **1b** and **1c** occur at 1761, 1252, and 1793, 1274 cm^{-1}, respectively. The ^{31}P NMR spectra of all three complexes display the same characteristic pattern of signals previously simulated and discussed.[15]

Table 3. Selected Intramolecular Distances and Angles Involving the Non-Hydrogen Atoms for [Ta(≡COSi^{t}BuPh$_2$)(CO)(dmpe)$_2$] (1b)[a]

Bond Distances			
Ta–P1	2.469(2)	Ta–P2	2.613(2)
Ta–P3	2.512(2)	Ta–P4	2.568(2)
Ta–C1	1.881(6)	Ta–C2	2.018(8)
C1–O1	1.364(7)	C2–O2	1.186(9)
Si–O1	1.667(5)		
Bond Angles			
Ta–C1–O1	168.3(5)	Ta–C2–O2	179.5(6)
C1–Ta–C2	89.1(3)	Si–O1–C1	127.1(4)
P1–Ta–P2	76.90(7)	P1–Ta–P3	172.73(6)
P1–Ta–P4	96.74(7)	P1–Ta–C1	85.0(2)
P1–Ta–C2	92.0(2)	P2–Ta–P3	99.85(7)
P2–Ta–P4	95.97(7)	P2–Ta–C1	159.2(2)
P2–Ta–C2	81.5(2)	P3–Ta–P4	77.01(6)
P3–Ta–C1	99.2(2)	P3–Ta–C2	94.0(2)
P4–Ta–C1	96.2(2)	P4–Ta–C2	170.1(2)

[a] Atoms are labeled as indicated in Figure 1. Distances are in angstroms and angles are in degrees. Estimated standard deviations in the least significant figure are given in parentheses.

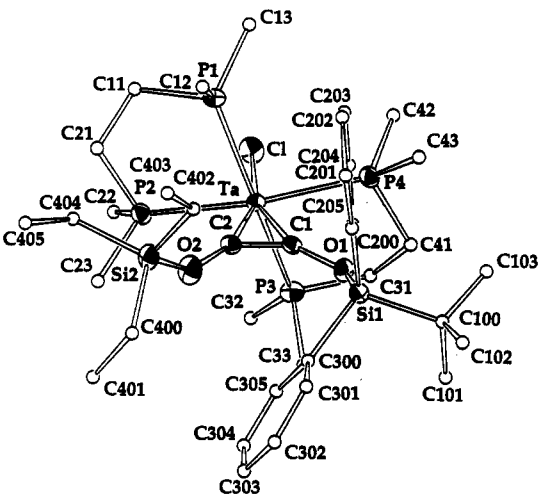

Figure 2. Structural diagram of [Ta(^{t}BuPh$_2$SiOC≡COSiEt$_3$)(dmpe)$_2$Cl] (**2d**) showing 40% thermal ellipsoids for selected atoms and, for clarity, 0.1-Å spheres for the remaining non-hydrogen atoms.

$$\text{Na[Ta(CO)}_2\text{(dmpe)}_2\text{]} + \text{R}_3\text{SiCl} \xrightarrow{\text{THF}} \text{[Ta(≡COSiR}_3\text{)(CO)(dmpe)}_2\text{]} \quad (3)$$

$$\text{R}_3\text{Si} = {}^i\text{Pr}_3\text{Si (1a)}, {}^t\text{BuPh}_2\text{Si (1b)}, \text{Ph}_3\text{Si (1c)}$$

(25) Vrtis, R. N.; Bott, S. G.; Lippard, S. J. *Organometallics* **1992**, *11*, 270.

(26) Protasiewicz, J. D.; Lippard, S. J. Unpublished results.

Table 4. Positional Parameters and B(eq) for [Ta(^{t}BuPh$_2$SiOC≡COSiEt$_3$)(dmpe)$_2$Cl] (2d)[a]

atom	x	y	z	B(eq),Å^2 [b]
Ta	0.84868(1)	0.14917(1)	0.28340(1)	1.461(8)
Cl	0.96441(7)	0.0188(1)	0.33586(7)	2.65(4)
P1	0.88749(7)	0.1502(1)	0.17919(7)	2.18(5)
P2	0.78428(7)	-0.0195(1)	0.21389(7)	2.07(4)
P3	0.84400(7)	0.1005(1)	0.40244(7)	2.23(5)
P4	0.95226(7)	0.2697(1)	0.37487(7)	2.13(4)
Si1	0.71265(7)	0.4836(1)	0.27293(7)	1.78(4)
Si2	0.60467(7)	0.2461(1)	0.08066(7)	2.46(5)
O1	0.7716(2)	0.3804(2)	0.3033(2)	2.1(1)
O2	0.6635(2)	0.2176(3)	0.1664(2)	3.2(1)
C1	0.7810(2)	0.2848(3)	0.2727(2)	1.6(1)
C2	0.7389(2)	0.2190(4)	0.2187(2)	1.8(2)
C11	0.8659(3)	0.0180(4)	0.1335(3)	2.9(2)
C12	0.8315(3)	0.2388(5)	0.1032(3)	3.7(2)
C13	0.9860(3)	0.1740(4)	0.1905(3)	3.1(2)
C21	0.7881(3)	-0.0242(4)	0.1240(3)	3.0(2)
C22	0.8251(3)	-0.1506(4)	0.2508(3)	3.2(2)
C23	0.6820(3)	-0.0440(4)	0.1881(3)	3.0(2)
C31	0.9285(3)	0.1572(4)	0.4813(3)	3.1(2)
C32	0.8453(4)	-0.0379(5)	0.4330(3)	4.0(2)
C33	0.7619(3)	0.1559(4)	0.4138(3)	2.9(2)
C41	0.9448(3)	0.2705(5)	0.4630(3)	3.4(2)
C42	1.0548(3)	0.2414(4)	0.4055(3)	2.9(2)
C43	0.9540(3)	0.4120(4)	0.3573(3)	3.3(2)
C100	0.7433(3)	0.5757(4)	0.3557(3)	2.4(2)
C101	0.7307(4)	0.5192(5)	0.4165(3)	4.1(2)
C102	0.6939(3)	0.6770(4)	0.3337(3)	3.1(2)
C103	0.8283(3)	0.6080(5)	0.3851(3)	3.9(2)
C200	0.7279(3)	0.5489(4)	0.1971(2)	2.2(2)
C201	0.7928(3)	0.5211(4)	0.1861(3)	2.7(2)
C202	0.8081(3)	0.5658(4)	0.1319(3)	3.4(2)
C203	0.7582(3)	0.6413(4)	0.0849(3)	3.3(2)
C204	0.6935(3)	0.6712(4)	0.0940(3)	3.1(2)
C205	0.6793(3)	0.6273(4)	0.1502(3)	2.7(2)
C300	0.6099(2)	0.4401(4)	0.2469(2)	1.9(2)
C301	0.5981(3)	0.3406(4)	0.2699(3)	2.8(2)
C302	0.5250(3)	0.3086(5)	0.2602(3)	3.7(2)
C303	0.4634(3)	0.3778(5)	0.2281(4)	3.7(2)
C304	0.4735(3)	0.4757(5)	0.2046(3)	3.7(2)
C305	0.5466(3)	0.5073(4)	0.2131(3)	3.0(2)
C400	0.5072(3)	0.2596(5)	0.0761(3)	3.9(2)
C401	0.4738(5)	0.1608(6)	0.0927(5)	6.3(4)
C402	0.6327(4)	0.3753(5)	0.0527(4)	4.8(3)
C403	0.5881(6)	0.4185(8)	-0.0195(5)	10.2(5)
C404	0.6015(3)	0.1377(4)	0.0158(3)	3.6(2)
C405	0.5320(4)	0.1426(5)	-0.0596(3)	5.4(3)

[a] Atoms are labeled as indicated in Figure 2. Estimated standard deviations in the last digit are given in parentheses. [b] B(eq) = $^4/_3[a^2\beta_{11} + b^2\beta_{22} + c^2\beta_{33} + 2ab\cos(\gamma)\beta_{12} + 2ac\cos(\beta)\beta_{13} + 2bc\cos(\alpha)\beta_{23}]$.

The structure of **1b**, determined in a single crystal X-ray study, is presented in Figure 1. Table 2 lists the fractional coordinates for this molecule and Table 3 summarizes important bond distances and angles. The geometry of **1b** is comparable to that determined previously for **1a** and [Nb(≡COSi^{i}Pr$_3$)(CO)(dmpe)$_2$].[15] For example, the metal–carbon distance for the carbyne ligand in **1a** is 1.85(1) Å (1.88(1) Å for the Nb analogue), whereas for **1b** the value is 1.881(1) Å. The average Ta–P bond length for both complexes is 2.54 Å. The C(1)–Ta–C(2) angle of 88.5(6)° in **1a** compares well to the value of 89.1(3)° determined for **1b**.

Addition of Me$_3$SiCl to **1a** yields the asymmetric acetylene complex [Ta(Me$_3$SiOC≡COSi^{i}Pr$_3$)(dmpe)$_2$Cl] (**2a**).[15] Carbynes **1b** and **1c** also react with Me$_3$SiCl and Et$_3$SiCl in a similar manner (eq 4). These complexes can be isolated as green-brown crystalline materials by recrystallization from pentane at −30 °C. A characteristic $\nu_{C\equiv C}$ stretch is observed at about 1560–1570 cm^{-1} in the IR spectrum of **2a–d**. In addition, each complex shows a single resonance for its ^{31}P NMR spectrum at room temperature, indicating facile rotation of the acetylene about the vector connecting the metal and midpoint of the C—C bond. Such behavior is common for 4 e$^-$ donating acetylenes.[27]

Table 5. Selected Intramolecular Bond Distances and Angles Involving the Non-Hydrogen Atoms for [Ta(Et$_3$SiOC≡COSi^{t}BuPh$_2$)(dmpe)$_2$Cl] (2d)[a]

Bond Distances			
Ta–P1	2.526(1)	Ta–P2	2.535(1)
Ta–P3	2.522(1)	Ta–P4	2.535(1)
Ta–C1	2.092(4)	Ta–C2	2.123(4)
Ta–C1	2.583(1)	C1–C2	1.321(6)
C1–O1	1.394(5)	C2–O2	1.371(5)
Si1–O1	1.648(3)	Si2–O2	1.639(4)
Bond Angles			
Ta–C1–O1	147.8(3)	Ta–C2–O2	154.2(3)
C1–Ta–C2	36.5(2)	Si1–O1–C1	135.1(3)
Si2–O2–C2	144.9(3)		
C1–Ta–P1	80.05(4)	C1–Ta–P2	79.96(4)
C1–Ta–P3	80.93(4)	C1–Ta–P4	79.39(4)
C1–Ta–C1	160.1(1)	C1–Ta–C2	163.1(1)
P1–Ta–P2	78.13(4)	P1–Ta–P3	160.87(4)
P1–Ta–P4	100.29(4)	P1–Ta–C1	108.0(1)
P1–Ta–C2	93.7(1)	P2–Ta–P3	96.53(4)
P2–Ta–P4	159.24(4)	P2–Ta–C1	119.1(1)
P2–Ta–C2	83.6(1)	P3–Ta–P4	78.14(4)
P3–Ta–C1	90.7(1)	P3–Ta–C2	104.1(1)
P4–Ta–C1	81.3(1)	P4–Ta–C2	117.1(1)

[a] Atoms are labeled as indicated in Figure 2. Distances are in angstroms and angles are in degrees. Estimated standard deviations in the least significant figure are given in parentheses.

$$[Ta(\equiv COSiR_3)(CO)(dmpe)_2] \xrightarrow[THF]{R'_3SiCl} [Ta(R_3SiOC\equiv COSiR'_3)(dmpe)_2Cl] \quad (4)$$

$R_3Si = {}^iPr_3Si$; $R'_3Si = Me_3Si$ (**2a**)

$R_3Si = {}^tBuPh_2Si$; $R'_3Si = Me_3Si$ (**2b**)

$R_3Si = Ph_3Si$; $R'_3Si = Me_3Si$ (**2c**)

$R_3Si = {}^tBuPh_2Si$; $R'_3Si = Et_3Si$ (**2d**)

The geometry at the tantalum center in [Ta(Et$_3$SiOC≡COSi^{t}BuPh$_2$)(dmpe)$_2$Cl] (**2d**) is very similar to that observed for other seven-coordinate tantalum acetylene complexes, including **2a**. Figure 2 shows an ORTEP of the structure, and Tables 4 and 5 give the fractional coordinates and the important bond distances and angles, respectively. The average Ta—C bond distance of 2.112 Å is very similar to the value of 2.110 Å found in **2a**, and the C≡C bond distance of 1.321(6) Å in **2d** is equivalent to that found in **2a**. The average Ta—P bond distance of 2.530 Å, as well as the Ta—Cl distance of 2.583(1) Å, is within the range that has been previously observed for these complexes. Finally, the C1—Ta—C2 bond angle of 36.5(2)° is the same as in **2a**.

Kinetics Investigation of the Reductive Coupling Reaction. As previously mentioned, coupling of the carbyne and CO ligands in [M(≡COSiR$_3$)(CO)(dmpe)$_2$] complexes (M = group V metal) could possibly be promoted by either electrophiles or nucleophiles. To address this issue, we determined the kinetics of the reaction of **1a** with Me$_3$SiCl, a coupling reaction that was chosen for several reasons. Firstly, conversion to the product is quantitative and slow at room temperature in THF. Secondly, preparation of siloxycarbyne complexes of tantalum with less sterically encumbered silyl groups

(27) Templeton, J. L. *Adv. Organomet. Chem.* **1989**, *29*, 1.

Scheme 5

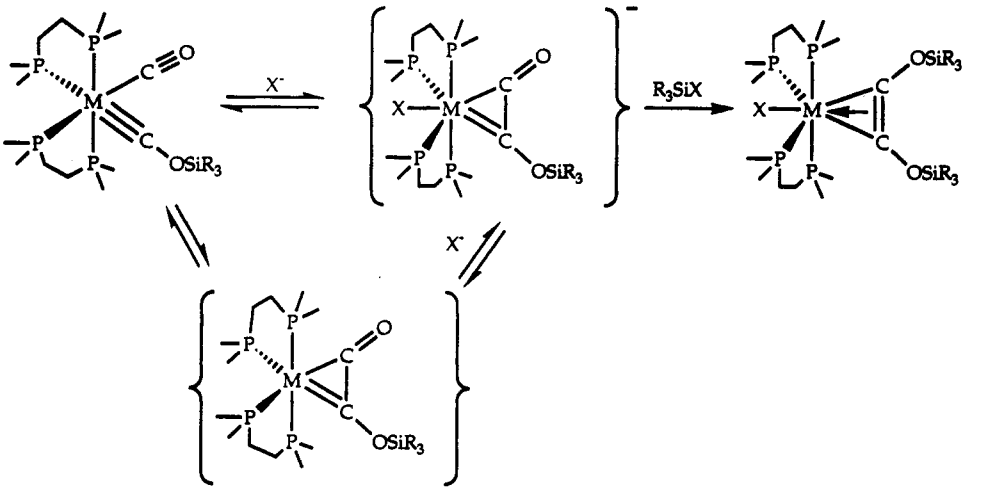

Scheme 6

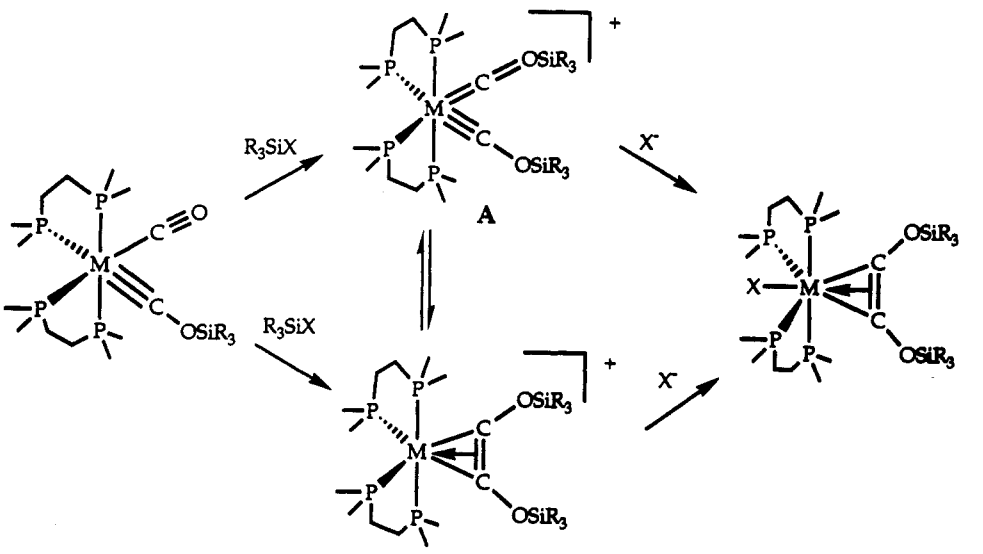

such as Me_3Si or Me_2PhSi led to the formation of dinuclear species. Finally, the corresponding vanadium carbynes proved difficult to isolate, and their coupled products were much more sensitive to traces of water and oxygen than the tantalum analogues.

If the rate-determining step in the reductive coupling were to require nucleophilic addition to the metal center to form an η^2-ketenyl intermediate (Scheme 5), then the reaction rate should depend on the concentration of added nucleophile. Conversely, if the rate-determining step involved electrophilic addition to the oxygen atom of the carbonyl ligand, then no such dependence should occur (Scheme 6). To distinguish between these possibilities, we measured rates of the coupling reaction in the presence and absence of $(n\text{-pentyl})_4NCl$, which provided chloride ion as a potential nucleophile. This ion could presumably be generated from Me_3SiCl during the coupling reaction.

Reactions of **1a** with Me_3SiCl were readily monitored in a stopped-flow device by visible spectroscopy, the color of **1a** being deep red whereas **2b** is green. In the absence of added tetraalkylammonium chloride, the reaction of **1a** and excess Me_3SiCl was quite slow, requiring several hours for completion. As the ionic strength of the solution was increased, however, the reaction rate accelerated, requiring the use of the stopped-flow spectrophotometer

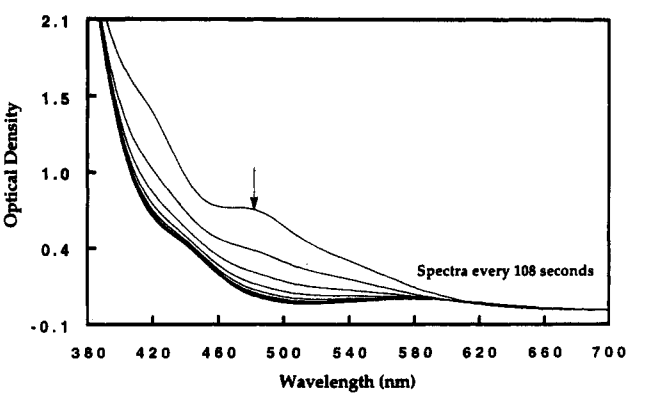

Figure 3. Spectral changes occurring upon mixing in the stopped-flow spectrophotometer of **1a** (3.8 mM) with Me_3SiCl (55.3 mM) in the presence of 32.9 mM $(n\text{-pentyl})_4NCl$ in THF.

to measure the kinetic parameters. The spectral changes for the red to green transformation were recorded by a diode-array spectrophotometer, as indicated for one set of conditions in Figure 3. Kinetic traces were obtained by following the change in optical density at 480 nm with the use of a fast fiber-optics detection system, which provided more data points per run. In this manner, the maximum

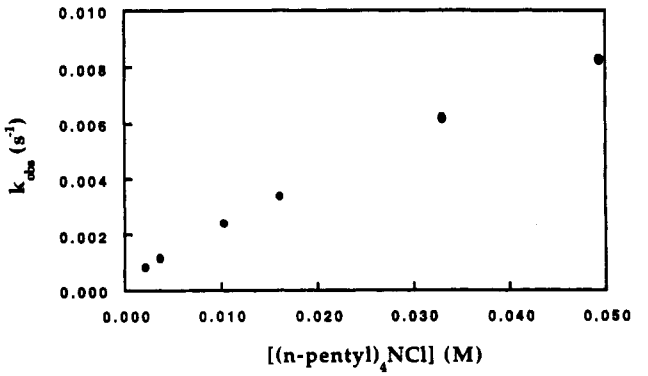

Figure 4. Effect of added (*n*-pentyl)$_4$NCl on k_{obs} for the reaction of **1a** with Me_3SiCl in THF (see Table 6 for details).

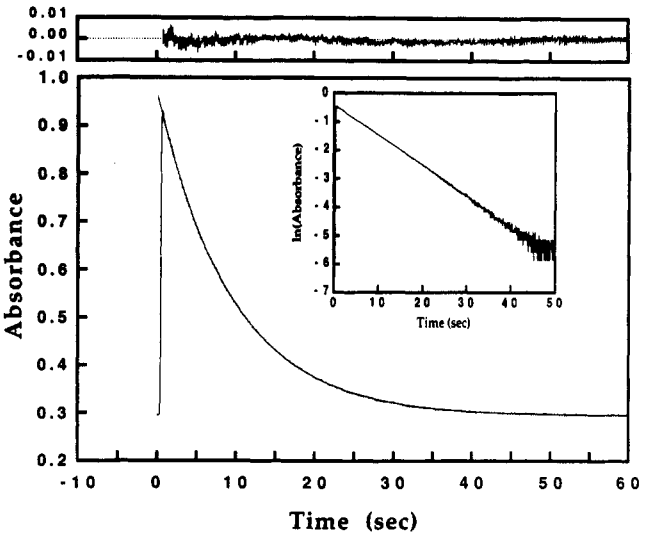

Figure 5. Kinetic traces obtained at 480 nm for the reaction of **1a** (4.5 mM) with Me_3SiCl (70.9 mM) in the presence of 24 mM nBu_4NBPh_4 in THF. The upper trace is residuals from the nonlinear fitting of the exponential curve, and the inset is the linearized form of the exponential curve. The observed and calculated traces are both displayed.

absorbance change in the visible range of the spectrum was recorded.

Addition of increasing amounts of (*n*-pentyl)$_4$NCl to the reaction medium led to substantial increases in k_{obs}, as shown in Table 6 and depicted graphically in Figure 4. This result initially suggested that chloride binding was occurring in the rate-determining step and that the reaction proceeded by the pathway depicted in Scheme 5. The relationship between k_{obs} and [(*n*-pentyl)$_4$NCl] was not linear, however, and a plot of ln(V_0) vs ln([(*n*-pentyl)$_4$NCl]) led to an apparent reaction order of 0.74 for (*n*-pentyl)$_4$NCl. In addition, examination of the reaction products obtained in the presence of (*n*-pentyl)$_4$NCl, surprisingly, revealed only [Ta($Me_3SiOC{\equiv}CO$-$SiMe_3$)(dmpe)$_2$Cl], and not **2a**. These two unexpected phenomena could be understood when the reaction was run with (*n*-butyl)$_4$NBPh$_4$ rather than (*n*-pentyl)$_4$NCl. Interestingly, the rates observed in the presence of the BPh_4^- salt were even greater than those for the chloride salt. Figure 5 shows the trace of absorbance versus time for one such run, revealing that the reaction was complete in under 60 s. Moreover, no such scrambling of the silyl groups occurred in the presence of the (*n*-butyl)$_4$NBPh$_4$ salt; only **2a** formed under these conditions.

Such large rate enhancements with an increase in the ionic strength or dielectric constant of the reaction medium

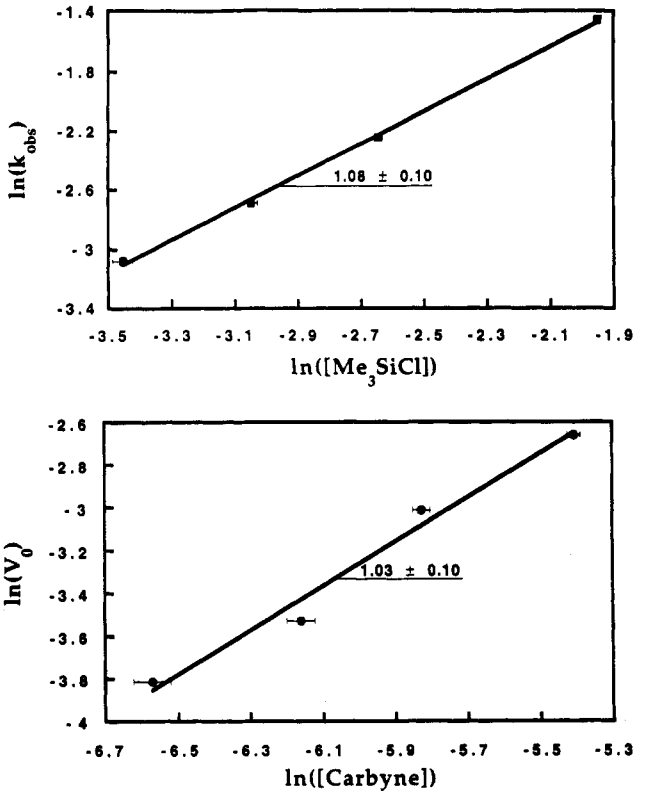

Figure 6. Reaction order plots for Me_3SiCl (above) and **1a** (below).

are consistent with reaction of **1a** and Me_3SiCl to form a charged intermediate or transition state.[28,29] Salt effects are expected to be large for solvents of low polarity.[30,31] Such large kinetic salt effects do not appear to have been reported for organometallic complexes, in contrast to the wealth of such data available for organic reactions.[32,33] The importance of ion pairing effects for transition metal complexes, however, has been noted, especially with respect to the altered lability of coordinated ligands.[34,35] Similar rate enhancements have been obtained by changes to more polar solvents. For example, charged intermediates have been inferred from the large solvent effects on the rates of oxidative addition of alkyl halides to d^8 transition metal complexes.[36,37] Salt effects on electron transfer rates have also been measured for organometallic complexes, but much smaller rate differences were determined.[38]

(28) Conners, K. A. *Chemical Kinetics. The Study of Reaction Rates in Solution*; VCH Publishers Inc.: New York, 1990.
(29) Zuman, P.; Patel, R. C. *Techniques in Organic Reaction Kinetics*; John Wiley & Sons: New York, 1984.
(30) Loupy, A.; Tchoubar, B.; Astruc, D. *Chem. Rev.* **1992**, *92*, 1141.
(31) Conductivity data for (*n*-butyl)$_4$NBPh$_4$ in THF could not be located, but for results for salts containing one of the two ions in THF see: (a) Bhattacharyya, D. N.; Lee, C. L.; Smid, J.; Szwarc, M. *J. Phys. Chem.* **1965**, *69*, 608. (b) Boileau, S.; Hemery, P.; Justice, J.-C. *J. Solution Chem.* **1975**, *4*, 873. (c) Boileau, S.; Hemery, P. *Electrochim. Acta* **1976**, *21*, 647. (d) Sigvartsen, T.; Gestblom, B.; Noreland, E.; Songstad, J. *Acta Chem. Scand.* **1989**, *43*, 103. For conductivity data for (*n*-butyl)$_4$NBPh$_4$ in 2-chloromethyl–THF see: Salomon, M. *Electrochim. Acta* **1985**, *30*, 1021.
(32) Lowry, T. H.; Richardson, K. H. *Mechanism and Theory in Organic Chemistry*, 2nd ed.; Harper & Row: New York, 1981.
(33) *Ions and Ion pairs in Organic Reactions*; Szwarc, M., Ed.; Wiley-Interscience: New York, 1972; Vols. 1 & 2.
(34) Darensbourg, M. Y. *Prog. Inorg. Chem.* **1985**, *33*, 221.
(35) Kochi, J. K.; Bockman, T. M. *Adv. Organomet. Chem.* **1991**, *33*, 51.
(36) Hart-Davis, A. J.; Graham, W. A. G. *Inorg. Chem.* **1970**, *9*, 2658.
(37) Stille, J. K.; Lau, K. S. Y. *Acc. Chem. Res.* **1977**, *10*, 434.
(38) For example, see: (a) Anderson, K. A.; Wherland, S. *Inorg. Chem.* **1989**, *28*, 601. (b) Chan, M.-S.; Wahl, A. C. *J. Phys. Chem.* **1982**, *86*, 126.

Table 6. Rate Data for Reaction of 1a with Me_3SiCl in THF at 22 ± 1 °C[a]

[1a]	[Me_3SiCl]	[(n-pentyl)$_4$NCl]	[(n-butyl)$_4$NBPh$_4$]	10^2k_{obs} (s^{-1})	10^2V_0 (Abs·s^{-1})
			1. Halide Effect		
3.0	55.3	2.1	0.0	0.08 ± 0.01	
"	"	3.6	"	0.12 ± 0.02	
"	"	10.2	"	0.24 ± 0.01	
"	"	16.0	"	0.34 ± 0.01	
"	"	33.0	"	0.62 ± 0.02	
"	"	49.3	"	0.83 ± 0.02	
			2. Salt Effect		
3.0	70.9	5.8	23.9	6.14 ± 0.07	
"	"	0.0	23.9	10.65 ± 0.05	
"	"	0.0	29.8	13.67 ± 0.09	
			3. Order versus [Me_3SiCl]		
3.0	31.6	0.0	23.9	4.60 ± 0.21	
"	47.4	"	"	6.82 ± 0.06	
"	70.9	"	"	10.64 ± 0.06	
"	142.2	"	"	23.33 ± 0.06	
			4. Order versus [1a]		
1.4	70.9	0.0	23.9		2.21 ± 0.01
2.1	"	"	"		2.93 ± 0.02
2.9	"	"	"		4.92 ± 0.03
4.5	"	"	"		7.00 ± 0.07

[a] Concentrations are in mM.

At a constant total salt concentration of 29.8 mM the rate constant was slightly higher for pure (n-butyl)$_4$NBPh$_4$ compared to a mixture of 23.9 mM (n-pentyl)$_4$NCl and (n-butyl)$_4$NBPh$_4$ (5.8 mM), Table 6. The slight rate decrease in the presence of chloride ion could be due to the scrambling effect, discussed further below. Alternatively, mixed ion pairing among the four different charged species might have resulted in a different ionic strength for the two experiments. Catalysis of nucleophilic reactions at tetravalent silicon compounds R_3SiX by nucleophiles such as F^-, HMPA, and $RCOO^-$ has been reported, but chloride does not appear to act in a similar manner.[39]

At a constant (n-butyl)$_4$NBPh$_4$ concentration of 23.9 mM, first order behavior was obtained for the reaction of **1a** with Me_3SiCl, Figure 6. A second order rate constant of 1.71 ± 0.04 M^{-1} s^{-1} at 22 ± 1 °C was obtained under these conditions. These and the foregoing results are consistent with a rate-determining step involving electrophilic attack of the silyl reagent on the CO ligand of **1a** (Scheme 6). Another formal mechanistic possibility, not excluded on the basis of the kinetic results alone, is that **1a** is in rapid equilibrium with an electronically unsaturated η^2-ketenyl complex, which is then trapped by Me_3SiCl to generate species such as **2a** (eq 5). We do not believe

$$[Ta(\equiv COSi^iPr_3)(CO)(dmpe)_2] \rightleftharpoons [Ta(\eta^2\text{-}O{=}CCOSi^iPr_3)(dmpe)_2] \xrightarrow{Me_3SiCl} \mathbf{2a} \quad (5)$$

this pathway to be operative for several reasons. Addition of nucleophiles to **1a** has never resulted in trapping of a ketenyl complex. The dmpe ligands donate considerable electron density to the metal center, making ligand addition to the already electron-rich site less favorable. Furthermore, addition of AlR_3 to **1** did not result in formation of acetylene complexes (see below).

The chloride-induced scrambling of silyl groups described above also indicates that the site of nucleophilic attack in these complexes is at the silicon atom rather than the metal atom. A mechanism that explains the scrambling is depicted in Scheme 7. The proposed equilibrium involving **1a** and chloride ion must lie far to the left, however, since $[Ta(CO)_2(dmpe)_2]^-$ was not detected by ^1H and ^{31}P NMR spectroscopy when excess (n-pentyl)$_4$NCl or NaCl was added to a THF solution of **1a**. Addition of 1 equiv of Me_3SiCl to a THF-d_8 solution of **1a** in the presence of 0.1 equiv of (n-pentyl)$_4$NCl led to the immediate formation of free $^iPr_3SiCl$ and a new complex, the ^1H and ^{31}P NMR properties of which were consistent with the formation of the Me_3Si-substituted carbyne complex (eq 6). Desilylation was observed as the main reaction, albeit occurring very slowly, over a period of weeks when **1a** was allowed to react with KO^{t}Bu in THF (eq 7).

Scheme 7

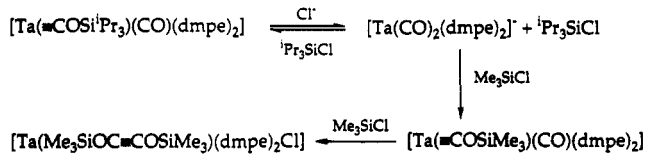

$$[Ta(\equiv COSi^iPr_3)(CO)(dmpe)_2] \xrightarrow[\text{cat. } Cl^-]{Me_3SiCl} [Ta(\equiv COSiMe_3)(CO)(dmpe)_2] + {}^iPr_3SiCl \quad (6)$$

$$[Ta(\equiv COSi^iPr_3)(CO)(dmpe)_2] \xrightarrow{KO^tBu} K[Ta(CO)_2(dmpe)_2] + {}^tBuOSi^iPr_3 \quad (7)$$

Scrambling of the silyl groups could occur from other species during the reaction. Control experiments showed that reaction of **2a** or **2b** with Me_3SiCl in the presence of (n-pentyl)$_4$NCl in THF occurred only slowly (days to weeks) to form [Ta(Me$_3$SiOC≡COSiMe$_3$)(dmpe)$_2$Cl], a reaction much too slow to account for scrambling observed during the present experiments. Scrambling from either **A** or **B** in Scheme 6 seems unlikely, since removal of Me_3Si^+ by the chloride ion should be favored over removal of $^iPr_3Si^+$, on the basis of steric arguments. Removal of Me_3Si^+ would re-form **1a**, resulting in a nonproductive reversal of the silylation reaction. This chemistry would explain why the rate decreased in the presence of chloride at a

(39) Corriu, R. J. P.; Guerin, C.; Henner, B. J. L.; Man, W. W. C. W. C. *Organometallics* **1988**, *7*, 237.

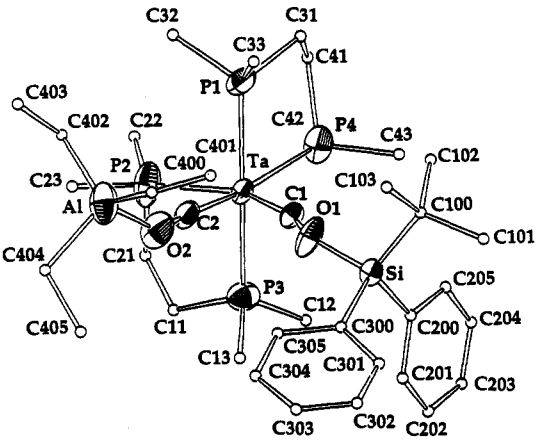

Figure 7. Structural diagram of [Ta(≡COSi^{t}BuPh$_2$)(COAlEt$_3$)(dmpe)$_2$] (**3b**) showing 30% thermal ellipsoids for selected atoms and, for clarity, 0.1-Å spheres for the remaining non-hydrogen atoms. A full ORTEP diagram is provided with the supplementary material for ref 23.

constant salt concentration, as discussed above. Moreover, no evidence of silyl group scrambling was observed in the presence of (n-butyl)$_4$NBPh$_4$, which might be expected if such a process were occurring.

Synthesis and Properties of Carbene–Carbyne Complexes. Electrophilic attack of the silyl reagent on the CO ligand of **1a** can generate two possible intermediates, **A** or **B**, as depicted in Scheme 6. The kinetic experiments by themselves do not distinguish these alternatives since the C—C bond-forming step can occur during or after the rate-determining step. The related reaction of Me$_3$SiOTf with Na[V(CO)$_2$(dmpe)$_2$] yields [V(Me$_3$SiOC≡COSiMe$_3$)(dmpe)$_2$]OTf, which might imply that coupling occurs concomitantly with silylation of the intermediate carbyne–CO complex.[21] To separate the roles of anion and electrophile from one another in the coupling process of the corresponding tantalum complexes, we have explored reactions of **1a** with trialkylaluminum reagents.

Addition of 1 equiv of either AlMe$_3$ or AlEt$_3$ to a toluene solution of **1a** immediately converted the deep red color of **1a** to a light orange-red. The IR spectrum of the reaction product showed that ν_{CO} of **1a** had shifted dramatically from 1805 to 1611 cm^{-1} in the AlEt$_3$ derivative. Although the latter value is in the range for ν_{CC} in coordinated disiloxyacetylenes, the strong intensity of the absorption suggested that it might be due to a CO stretching mode.

Similar products were obtained with complexes **1b** and **1c**. X-ray quality crystals of the **1b**·AlEt$_3$ (**3b**) adduct were grown, and its crystal structure was determined. An ORTEP representation of the molecular geometry is shown in Figure 7. Table 7 lists atomic coordinates whereas important bond angles and distances for **3b** are provided in Table 8. As inferred from the IR spectrum, electrophilic addition of AlEt$_3$ did not result in coupling of the carbyne and CO ligands, although the structure of the resulting complex has several interesting attributes.

The Ta–C2 distance in **3b** is 1.93(1) Å, considerably shorter than the corresponding distance in **1b**, 2.018(8) Å. This result indicates an increase in the Ta–C2 bond order. A corresponding decrease in the C–O bond order occurs for the CO ligand, the C2–O2 bond distance lengthening from 1.186(9) Å in **1b** to 1.23(1) Å in **3b**. The metal–carbon triple bond has similarly undergone a slight lengthening to 1.894(9) Å in **3b** from 1.881(6) Å in **1b**, and the C1–O1 distances have shortened to 1.32(1) Å in **3b** from 1.365(7) Å in **1b**. Attenuation of the CO bond lengths in going from **1b** to **3b** are paralleled by the changes in the IR spectra of these compounds. The CO stretches of **1b** appear at 1793 and 1274 cm^{-1} (1749 and 1237 cm^{-1} for the doubly-^{13}C-labeled derivative), whereas those of **3b** appear at 1579 and 1321 cm^{-1} (1540 and 1285 cm^{-1} for the doubly-^{13}C-labeled derivative).

Table 7. Positional Parameters and B(eq) for [Ta(≡COSi^{t}BuPh$_2$)(COAlEt$_3$)(dmpe)$_2$] (3b)[a]

atom	x	y	z	B(eq), Å^2 [b]
Ta	0.11158(2)	0.12226(3)	0.63700(1)	3.63(2)
P1	0.0827(1)	0.2021(3)	0.5653(1)	6.2(1)
P2	–0.0102(2)	0.0683(3)	0.6111(1)	8.3(2)
P3	0.1269(2)	0.0557(2)	0.7107(1)	5.5(1)
P4	0.0863(2)	0.2806(2)	0.6782(1)	6.7(2)
Si1	0.3250(1)	0.1745(2)	0.63144(8)	3.8(1)
Al1	0.1739(2)	–0.2139(3)	0.6125(2)	8.1(2)
O1	0.2611(3)	0.1091(4)	0.6364(3)	6.4(4)
O2	0.1570(5)	–0.0781(6)	0.6023(3)	8.3(5)
C1	0.2022(4)	0.1298(6)	0.6404(3)	3.9(4)
C2	0.1351(5)	–0.0028(7)	0.6150(3)	5.0(5)
C11	–0.0024(8)	0.166(2)	0.5345(5)	18(2)
C12	0.081(1)	0.336(1)	0.5605(6)	13(1)
C13	0.1321(7)	0.167(1)	0.5305(4)	8.6(8)
C21	–0.049(1)	0.138(2)	0.560(1)	19(1)
C22	–0.0764(9)	0.096(2)	0.633(1)	22(2)
C23	–0.0268(7)	–0.060(1)	0.5948(5)	10.0(9)
C31	0.129(1)	0.152(1)	0.7499(4)	10(1)
C32	0.0654(8)	–0.030(1)	0.7212(5)	9.9(9)
C33	0.2021(6)	–0.012(1)	0.7341(4)	8.0(7)
C41	0.076(1)	0.232(1)	0.7316(5)	11(1)
C42	0.0152(7)	0.360(1)	0.6637(5)	9.8(9)
C43	0.1531(7)	0.3693(8)	0.6936(4)	7.2(6)
C100	0.3833(5)	0.1805(9)	0.6857(4)	6.0(5)
C101	0.4405(7)	0.253(1)	0.6861(4)	9.5(8)
C102	0.3458(7)	0.219(1)	0.7180(4)	9.0(8)
C103	0.4081(7)	0.076(1)	0.6995(4)	8.6(7)
C200	0.2986(4)	0.2992(7)	0.6073(3)	4.5(4)
C201	0.2940(5)	0.3159(8)	0.5647(4)	6.1(6)
C202	0.2712(7)	0.405(1)	0.5449(4)	7.5(7)
C203	0.2528(7)	0.480(1)	0.5664(6)	8.3(8)
C204	0.2566(7)	0.4686(9)	0.6085(5)	8.1(7)
C205	0.2798(6)	0.3773(8)	0.6293(4)	6.4(6)
C300	0.3601(5)	0.0989(7)	0.5948(3)	4.7(4)
C301	0.4171(6)	0.1261(9)	0.5844(4)	6.3(6)
C302	0.4427(8)	0.072(1)	0.5579(5)	9(1)
C303	0.414(1)	–0.013(2)	0.5399(5)	11(1)
C304	0.356(1)	–0.043(1)	0.5478(5)	10(1)
C305	0.3283(7)	0.0121(9)	0.5758(4)	7.1(6)
C400	0.268(1)	–0.229(1)	0.6391(8)	20(2)
C401	0.307(1)	–0.164(2)	0.6647(8)	15(1)
C402	0.112(1)	–0.258(1)	0.643(1)	22(2)
C403	0.115(1)	–0.361(2)	0.6565(9)	16(2)
C404	0.144(1)	–0.267(1)	0.5554(9)	18(2)
C405	0.185(1)	–0.216(2)	0.5264(8)	18(2)

[a] Atoms are labeled as indicated in Figure 7. Estimated standard deviations in the last digit are given in parentheses. [b] B(eq) = $^4/_3[a^2\beta_{11} + b^2\beta_{22} + c^2\beta_{33} + 2ab\cos(\gamma)\beta_{12} + 2ac\cos(\beta)\beta_{13} + 2bc\cos(\alpha)\beta_{23}]$.

The ^{31}P NMR spectral properties of **1b** and **3b** are very similar except for the 8 ppm upfield shift for one of multiplets of the phosphine atoms. This envelope is tentatively assigned to the dmpe phosphorus atom trans to the aluminum-derivatized CO ligand. Comparison of the ^{13}C NMR spectra (C_6D_6) of the doubly-^{13}C-labeled species **1b*** and **3b*** shows that the ^{13}C resonances of **1b*** (δ 240.8 and 253.8) have moved downfield in **3b*** to δ 247.4 and 267.0. Both species gave broad signals, and no coupling information was obtained. Lewis acid adducts of CO ligands typically shift noticeably downfield compared to the corresponding carbon atom of the CO ligand in the parent complex.[40] The larger, δ 253.8 to 267.0, shift of the ^{13}C NMR resonances was therefore assigned to the

Table 8. Selected Intramolecular Bond Distances and Angles Involving the Non-Hydrogen Atoms for [Ta(≡COSi^{t}BuPh$_2$)(COAlEt$_3$)(dmpe)$_2$] (3b)^a

Bond Distances			
Ta–P1	2.508(3)	Ta–P2	2.595(3)
Ta–P3	2.515(3)	Ta–P4	2.637(3)
Ta–C1	1.894(9)	Ta–C2	1.93(1)
C1–O1	1.32(1)	C2–O2	1.23(1)
Si–O1	1.652(7)	Al–O2	1.862(9)
Bond Angles			
Ta–C1–O1	162.4(7)	Ta–C2–O2	172.8(9)
C1–Ta–C2	73.4(4)	Si–O1–C1	135.9(6)
Al–O2–C2	144.1(8)		
P1–Ta–P2	80.4(1)	P1–Ta–P3	171.8(1)
P1–Ta–P4	96.1(1)	P1–Ta–C1	91.6(3)
P1–Ta–C2	92.4(3)	P2–Ta–P3	94.8(1)
P2–Ta–P4	94.2(1)	P2–Ta–C1	159.6(3)
P2–Ta–C2	88.2(3)	P3–Ta–P4	77.6(1)
P3–Ta–C1	95.0(3)	P3–Ta–C2	94.1(3)
P4–Ta–C1	105.3(3)	P4–Ta–C2	171.5(3)

^{a} Atoms are labeled as indicated in Figure 7. Distances are in angstroms and angles are in degrees. Estimated standard deviations in the least significant figure are given in parentheses.

$COAlEt_3$ moiety. This assignment requires the other ^{13}C signal of **1b** to arise from the carbyne carbon atom. Attempts to provide support for these assignments by preparing [Ta(≡*COSi^{t}BuPh$_2$)(CO)(dmpe)$_2$] from ^{12}CO and [Ta(≡*COSi^{t}BuPh$_2$)(*CO)(dmpe)$_2$] via thermal or photochemical methods were unsuccessful, however.

The most surprising feature of the solid state structure of **3b** is the C1—Ta—C2 bond angle of 73.4(4)°, which is 15.7° less than the same angle in **1b**. This deformation occurs without any significant change in the {Ta(dmpe)$_2$} core geometry between the two structures. The C1—C2 distance in **3b** is only 2.29(1) Å as a result of this distortion from octahedral geometry, compared to the C1—C2 distance of 2.74(1) Å in **1b**. It is possible that, for electronic reasons, the ligands in **3b** are trying to couple, but for steric reasons are unable to do so. To test this possibility, we showed (see above) that [Ta(Et$_3$SiOC≡COSi^{t}BuPh$_2$)(dmpe)$_2$Cl] could be prepared by reacting **1b** with Et_3SiCl. The steric requirements of $AlEt_3$ and Et_3Si should be very similar. In addition, [Ta(Et$_3$SiOC≡COSi^{t}BuPh$_2$)(dmpe)$_2$Cl] contains an extra ligand, chloride, making this complex even more sterically congested than **3b**. Thus, it seems unlikely that **3b** is restrained from coupling by steric factors.

Distortions from octahedral geometry have been observed in several d^4 transition metal complexes. For example, the C–Mo–C angle in [Mo(CO)$_2$(S$_2$CN^{i}Pr$_2$)$_2$] is only 72°. Such species have been analyzed by EHMO methods by Hoffmann and co-workers.[41] These compounds show a distortion of more than one pair of ligands and have an electron count that is two fewer than the present example. It is interesting that other compounds having both alkylidene and alkylidyne ligands bonded to the same metal center have been structurally characterized, and in these examples the C–M–C angles are always greater than 90°.[42] This property was attributed to repulsion of the lone pairs in the two multiply bonded M–C fragments. Structural distortions by π-accepting ligands of the {ML$_4$} fragment in octahedral d^6 transition metal complexes have

Chart 1

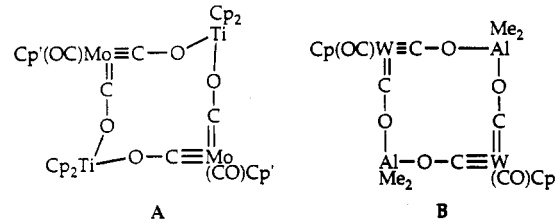

A B

also been explored by EHMO methods.[43] These observations provide no clear insight into the small C1–Ta–C2 bond angle in **3b**.

Another interesting feature of **3b** is the O2–Al bond distance of 1.861(9) Å, which is considerably longer than the O1–Si bond length of 1.652(7) Å. Based on the smaller covalent radius of aluminum versus silicon, one might have expected the Al–O distance to be shorter than the Si–O distance. These results indicate that the Al–O interaction in **3b** is substantially weaker than the Si–O interaction. This notion is borne out by the reactivity of **3b** with chloride in toluene solution, which did not effect coupling of the carbene and carbyne ligands. Instead, $AlEt_3$ was quantitatively removed and complex **1b** was formed. Removal of the $AlEt_3$ fragment was also observed when THF was added to these solutions, indicating the lability of the $AlEt_3$.

Adducts of CO ligands with aluminum and other Lewis acids are well-known.[40] They form with many electron-rich transition metal carbonyl complexes. The closest available structurally characterized carbene–carbyne complexes derived from CO ligands are shown in Chart 1.[44,45] The two sets of metal–carbon distances in **A** and **B** are 1.894, 1.865 and 1.88, 1.82 Å, respectively. The C–M–C angle for **A** is 88°, whereas for **B** it is 83.8(8)°. The cyclic structure of these two compounds may influence the C–M–C angle, so that comparisons with **3b** are hard to make. Neither of these two complexes undergoes coupling reactions of the type reported here.

Since formation of an aluminum–oxygen bond reagent has substantially diminished the metal–carbon bond length of the CO ligand, **3b** is best described as a carbene–carbyne complex (**X**, eq 8). Two alternative formulations, a bis-

(8)

(carbyne) (**Y**) or a bis(carbene) (**Z**) complex, are also depicted in eq 8. The bis(carbyne) formalism, although consistent with the common nomenclature that a CR fragment is a carbyne ligand, is not realistic due to the inability of a d-block transition metal to support two independent metal carbon triple bonds. Resonance form **Z**, the bis(carbene), is an acceptable alternative representation.

Isocyanide derived carbene–carbyne complexes were originally claimed to arise by double protonation of *trans*-[M(CNMe)$_2$(dppe)$_2$] (M = Mo and W, dppe = 1,2-bis(diphenylphosphino)ethane).[46] Recently, however, it has

(40) Horwitz, C. P.; Shriver, D. F. *Adv. Organomet. Chem.* **1984**, *23*, 219.
(41) Kubácek, P.; Hoffmann, R. *J. Am. Chem. Soc.* **1981**, *103*, 4320.
(42) Toreki, R.; Schrock, R. R.; Davis, W. M. *J. Am. Chem. Soc.* **1992**, *114*, 3367.
(43) Wink, D. J. *Organometallics* **1991**, *10*, 442.
(44) Merola, J. S.; Campo, K. S.; Gentile, R. A.; Modrick, M. A.; Zentz, S. *Organometallics* **1984**, *3*, 334.
(45) Conway, A. J.; Gainsford, G. J.; Schrieke, R. R.; Smith, J. D. *J. Chem. Soc., Dalton Trans.* **1975**, 2499.
(46) Chatt, J.; Pombeiro, A. J. L.; Richards, R. L. *J. Chem. Soc., Dalton Trans.* **1980**, 492.

Scheme 8

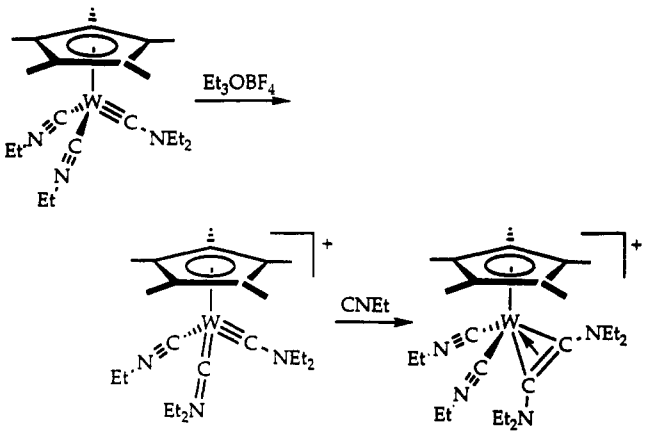

been found that the complexes had actually undergone reductive coupling, despite the trans configuration of the starting material.[47] Carbene–carbyne complexes have also been synthesized by ethylation of $[W(\equiv CNEt_2)(CNEt)_5]BF_4$ and $[Cp^*W(\equiv CNEt_2)(CNEt)_2]$ (Scheme 8).[19,48] Both of these carbene–carbene complexes yield coupled products upon addition of ligand.

Carbyne–CO coupling in these complexes is not restricted to organosilicon reagents. Recently, we have isolated coupled products of the form $[Ta(EtOC{\equiv}COSiR_3)(dmpe)_2OTf]$, as well as related derivatives, from the reaction of **1a** and **1b** with EtOTf.[49]

Conclusions

The kinetics of the reaction of $[Ta(\equiv COSi^iPr_3)(CO)(dmpe)_2]$ (**1a**) with Me_3SiCl in THF have been studied by stopped-flow visible spectroscopy. The reaction rate shows a first order dependence on both **1a** and Me_3SiCl. Large rate enhancements caused by added salts indicate that, during the rate-determining step, silylation of the CO ligand of **1a** occurs to yield a cationic intermediate. The nature of this intermediate has been probed by the addition of trialkylaluminum reagents to **1**. An X-ray structural analysis of $[Ta(\equiv COSi^tBuPh_2)(COAlEt_3)(dmpe)_2]$ (**3b**) reveals that the carbene and carbyne ligands have moved substantially toward one another, as required for C—C bond formation. In particular, the C—M—C angle decreased from 89.1(3)° in $[Ta(\equiv COSi^tBuPh_2)(CO)(dmpe)_2]$ (**1b**) to 73.4(4)° in **3b**. Coupling of these two unsaturated fragments is not prevented by steric interactions, as illustrated by the isolation and structural characterization of $[Ta(Et_3SiOC{\equiv}COSi^tBuPh_2)(dmpe)_2Cl]$ (**2d**), formed by reductive coupling chemistry.

Reaction of **1** with R_3SiX may involve bis(siloxy)carbene–carbyne complexes, but these species have been thus far unisolable in our system. We have also been able to isolate the isoelectronic bis(siloxy)acetylene complex $[V(Me_3SiOC{\equiv}COSiMe_3)(dmpe)_2]OTf$, suggesting that, in this case, coupling of any intermediate bis(siloxy)carbene–carbyne complex occurs spontaneously. Others have proposed that coupling of carbene and carbyne ligands should depend on the character of the carbene and carbyne ligands.[50] Ligands without stabilizing heteroatoms (X or Y) undergo spontaneous coupling to form a coordinated acetylene, thus shifting the equilibrium depicted in eq 9

(9)

to the right. Carbene–carbyne complexes are favored for groups that can delocalize the lone pair of electrons of the two carbyne ligands that do not find an orbital match at the metal center.[51–53] Our results suggest that the equilibrium between a carbene–carbyne complex and the corresponding acetylene complex will also depend on the choice of electrophile used to derivatize the heteroatom of the CO or CNR ligand. The $AlEt_3$ unit in $[Ta(\equiv COSi^tBuPh_2)(COAlEt_3)(dmpe)_2]$ is apparently bonded very weakly to the oxygen atom, and thus the aluminoxysiloxycarbene–carbyne complexes can be isolated. In the bis(siloxy) complexes, however, the interaction of the Si—O bonds are sufficiently strong such that they exist as acetylene complexes. Some isocyanide-derived carbene–carbyne complexes also appear to be stable species. The choice of metal center might also be important. We have been unable to obtain or detect any complex of the form $[Ta(R_3SiOC{\equiv}COSiR_3)(dmpe)_2]^+$ or $[Ta(\equiv COSiR_3)(COSiR_3)(dmpe)_2]^+$. Attempts to prepare such a complex by halide abstraction from $[Ta(R_3SiOC{\equiv}COSiR_3)(dmpe)_2Cl]$ by $TlPF_6$ led to the formation of paramagnetic $[Ta(R_3SiOC{\equiv}COSiR_3)(dmpe)_2Cl]PF_6$ complexes.[26]

Acknowledgment. This work was supported by a grant from the National Science Foundation. We are grateful to the George R. Harrison Spectroscopy Laboratory for allowing us access to their facility supported by NSF (CHE-8914953) and NIH (P41RR02594). A.M. thanks NATO, CIES, and the Human Frontier Science Program Organization for fellowships and research funding, and J.D.P. acknowledges support from Training Grant CA 09112 from the National Cancer Institute.

Supplementary Material Available: Full tables of bond distances and angles and positional and thermal parameters for **1b**, **2d**, and **3b** (25 pages). Ordering information is given on any current masthead page.

OM930692I

(47) Fraústo da Silva, J. J. R.; Pellinghelli, M. A.; Pombiero, A. J. L.; Richards, R. L.; Tiripicchio, A.; Wang, Y. *J. Organomet. Chem.* **1993**, *454*, C8.

(48) Filippou, A. C.; Völkl, C.; Grünleitner, W.; Kiprof, P. *J. Organomet. Chem.* **1992**, *434*, 201.

(49) Bronk, B. S.; Protasiewicz, J. D.; Lippard, S. J. Unpublished results.

(50) Mayr, A.; Bastos, C. M.; Daubenspeck, N.; McDermott, G. A. *Chem. Ber.* **1992**, *125*, 1583.

(51) Brower, D. C.; Templeton, J. L.; Mingos, D. M. P. *J. Am. Chem. Soc.* **1987**, *109*, 5203.

(52) Hoffmann, R.; Wilker, C. N.; Eisenstein, O. *J. Am. Chem. Soc.* **1982**, *104*, 632.

(53) Wilker, C. N.; Hoffmann, R.; Eisenstein, O. *Nouv. J. Chim.* **1983**, *7*, 535.